NMR Investigations of Orientational and Structural Changes in Polyamide-6 Yarns by Drawing

R. Schreiber and W. S. Veeman*

Department of Physical Chemistry, Lotharstrasse 1, 47057 University of Duisburg, Germany

W. Gabriëlse and J. Arnauts

DSM Research, P.O. Box 18, 6160 MD Geleen, The Netherlands

Received December 2, 1998

ABSTRACT: The effect of drawing on the structure and molecular orientation of polyamide-6 fibers has been investigated by ^{13}C solid-state NMR. The molecular orientation in the fibers is determined using a two-dimensional rotor synchronized magic-angle spinning (MAS) experiment. For the highly oriented fibers order parameters up to $\langle P_6 \rangle$ are determined. By using a ^{13}C $T_{1\rho}$ filter, the orientation in the rigid (crystalline + rigid amorphous) and mobile (amorphous) regions are separately determined. The orientation in the rigid phase increases rapidly at low draw ratios up to $\lambda = 3.5$ and levels off at higher draw ratios ($\langle P_2 \rangle \approx 0.75$). The mobile amorphous phase remains disordered for low draw ratios but orients rapidly for draw ratios above $\lambda = 3.5$. By using a ^{13}C T_1 filter, ^{13}C MAS spectra of the crystalline phase are obtained, from which the relative amounts of the α- and γ-phase can be quantitatively determined using spectral deconvolution. It appears that upon drawing the $^{\alpha}/_{\gamma}$ ratio changes from $^{60}/_{40}$ for an undrawn fiber to almost completely α for a fully drawn fiber. The NMR results are qualitatively supported by wide-angle X-ray spectroscopy (WAXS) photos.

1. Introduction

Polyamide-6 {poly[imino(1-oxo-1,6 hexanediyl)]} is a semicrystalline polymer in which the crystallites are embedded in an amorphous matrix.[1] Polyamide-6 fibers are industrially produced by the melt spinning process, followed by drawing. The physical properties of the fibers are affected by the process parameters, like the drawing ratio. In this paper, we study the effect of drawing on the polymer chain orientation and the crystalline structure of polyamide-6 fibers.

The morphology of polyamide-6 fibers has been investigated before by various techniques.[2−8] Recently, Murthy and Bray[5] investigated the effect of drawing on the polymer chain orientation of polyamide-6 fibers by X-ray diffraction, IR, and birefringence measurements. They were able to determine the chain orientation order parameter $\langle P_2 \rangle$ for the crystalline domains and for the oriented (anisotropic) part of the amorphous domains.

The structure and morphology of polyamide-6 has been studied by NMR (both ^{13}C and ^{15}N) by several groups.[9,10] The only NMR work on the chain orientation of polyamide-6 fibers was made by Tzou et al.[11] They performed NMR measurements on hot drawn polyamide-6 fibers and determined the average chain orientation parameters of the sample, i.e., averaged over the ordered crystalline and less-ordered amorphous domains.

Our primary goal is also to determine for drawn polyamide-6 fibers the chain orientation order parameters by ^{13}C solid-state NMR spectroscopy but, by using NMR filter methods, to separate the contributions of the amorphous and crystalline regions. ^{13}C NMR relaxation experiments are performed to study the phase structure of polyamide-6 and to separate amorphous and crystalline domains. In addition, we investigate by ^{13}C NMR the changes in crystal modification on drawing. Special attention is paid to the determination of the chemical shift tensor values, which are input parameters for the calculation of the orientational order parameters from the two-dimensional (2D) NMR spectra.

2. Experimental Section

2.1. Samples. A set of five round cross-sectional polyamide-6 fibers, all prepared by a melt spinning process were obtained from DSM (Geleen, The Netherlands). The polymer chips had a relative viscosity of 2.7 as measured in 98% sulfuric acid, and the temperature in the melt was 270 °C. The diameter of the spinning holes was 500 μm. The fibers were spun with a winding speed of 500 m/min and subsequently drawn to different draw ratios λ, i.e., 1.0 (undrawn), 2.0, 3.5, 4.0, and 4.5 in a separate step. The drawing temperature was 160 °C.

2.2. Sample Preparation. For the standard CPMAS and NMR relaxation experiments, the fibers were cut into short pieces and brought into the rotor. As discussed below, it appeared impossible to load the samples in such a way that no preferential orientation of the short pieces occurred.

For the NMR orientation experiments, the fibers are wound in a parallel way and first glued together to form a flat layer. A commercial available glue (UHU-Hart) that showed no signal overlap with the carbonyl resonance of polyamide-6 was used for this purpose. Furthermore, the glue did not contain water, which is thought to be important to avoid absorbance of water by polyamide-6. Then, 4−5 of these layers (dependent on the fiber thickness) were glued to a block. Finally, a block shape of approximately 4 × 4.5 × 11 mm has been cut in such a way that the fiber axis makes an angle of 60° with the rotor axis (see Figure 1). The empty spaces in the rotor are filled with talcum, to ensure stable spinning.

2.3. NMR Spectroscopy. The NMR measurements were performed on a Bruker ASX 400 spectrometer operating at 400 MHz for ^{1}H. A double-bearing CPMAS probe with 7 mm spinners was used. To obtain high resolution ^{13}C spectra, cross polarization (CP), high-power proton decoupling, and magic-angle spinning (MAS) have been applied. All spectra are referenced relative to adamantane (38.56 ppm for the methylene resonance relative to TMS).

The spinning frequency was 3500 Hz in all experiments, except for the orientation measurements (see below) which are

10.1021/ma9818679 CCC: $18.00
Published on Web 06/23/1999

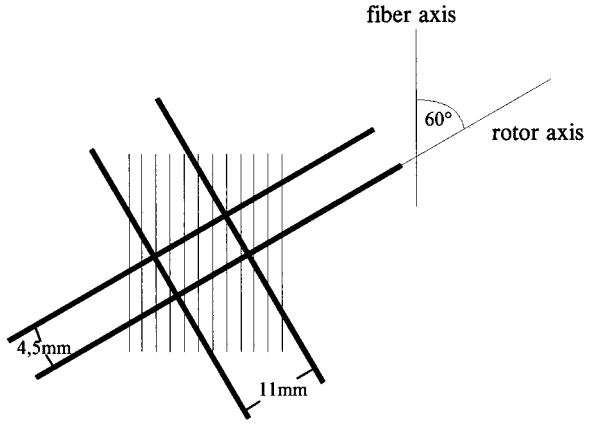

Figure 1. Scheme of sample preparation.

performed at 1750 Hz. The cross polarization time was 1 ms and the 90° pulse had a length of 5 μs in all experiments.

The ^{13}C rotorsynchronized 2D CPMAS experiment of Harbison et al.[12,13] (Figure 2a) was used to determine the chain orientation in terms of order parameters. Modification of this experiment by spin locking the carbons for 30 ms after cross polarization (^{13}C $T_{1\rho}$ filter) leads to a detection of the rigid phase only, due to the fast $T_{1\rho}$ relaxation of the carbons in the mobile phase (Figure 2b).

Under normal conditions, polyamide-6 absorbs water.[14−17] The T_g of polyamide-6 is strongly dependent on the water content. For dry polyamide-6 samples, T_g's of approximately 50 °C are reported.[18] At a water content of 4%, T_g is found at ca. 0 °C. Our fibers have a water content of approximately 2%. To ensure measuring conditions above T_g, all measurements were performed at a temperature of 40 °C.

3. Results and Discussion

3.1. Changes in Crystal Modification upon Drawing. Figure 3 shows the ^{13}C CPMAS spectrum of an undrawn polyamide-6 fiber and the assignment of the NMR signals. The CH_2 resonances occur in the range of 15−50 ppm and overlap strongly. This range includes resonances of the amorphous, α-, and γ-crystalline phases.[9,10] Some methylene carbons have a chemical shift which is sensitive to the crystalline modification, and therefore, a distinction of the different crystalline phases is possible. The assignments to the α- and γ-phases are indicated in the figure. Resonances of the amorphous phase, which are much broader than the crystalline resonances, are not separately visible.

The CH_2 resonances of polyamide-6 as a function of drawing are shown in Figure 4. The undrawn fiber shows resonances of both the α- and γ-crystalline phase. Upon drawing, the amount of the α-crystalline phase increases continuously, while the γ-crystalline phase nearly vanishes at high draw ratios. Deconvolution of these ^{13}C CPMAS spectra into separate peaks of the α-, γ-crystalline and amorphous phases was attempted. However, due to the strong overlap of the methylene resonances, a reliable fit could not be obtained. Thus, no quantitative information about the phase composition was obtained from these ^{13}C CPMAS spectra. The transformation of the γ- into the α-crystalline form upon drawing has been reported before.[5,7,8]

To quantify the relative amounts of the α- and γ-crystalline phases, the differences in ^{13}C T_1 relaxation times of the methylene carbons are used. The methylene carbons in the amorphous phase have a much shorter ^{13}C T_1 relaxation time (0.5−0.75 s[9]) than in the crystalline phase (10−20 s[9]). Therefore, a detection of only the crystalline parts is possible using a ^{13}C T_1 filter experiment. With a delay of 16 s, the amorphous CH_2 signals are strongly suppressed. The spectrum of the crystalline phase of the fiber drawn with a draw ratio of $\lambda = 4.5$, which is predominantly α, can easily be fitted with four α-phase peaks (see Figure 5a). The assignments as indicated in the figure are based on the assignments

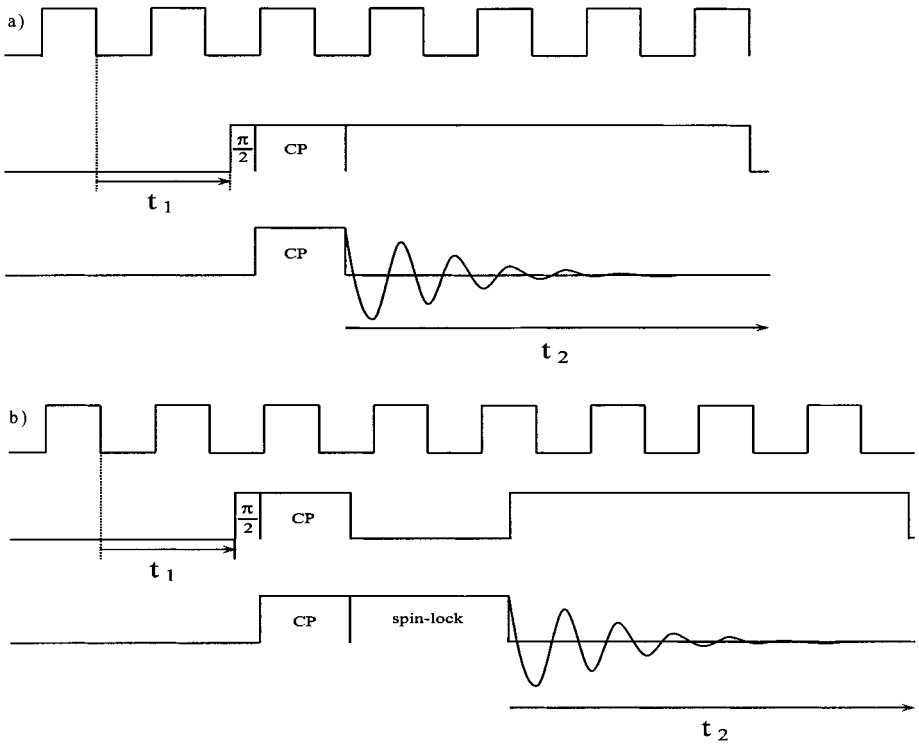

Figure 2. Schematic representation of pulse sequences used to obtain 2D spectra. (a) Rotorsynchronized 2D CPMAS experiment designed by Harbison et al.[12,13] (b) Rotorsynchronized 2D CPMAS experiment with additional spin-lock pulse used to obtain spectra of the rigid phase.

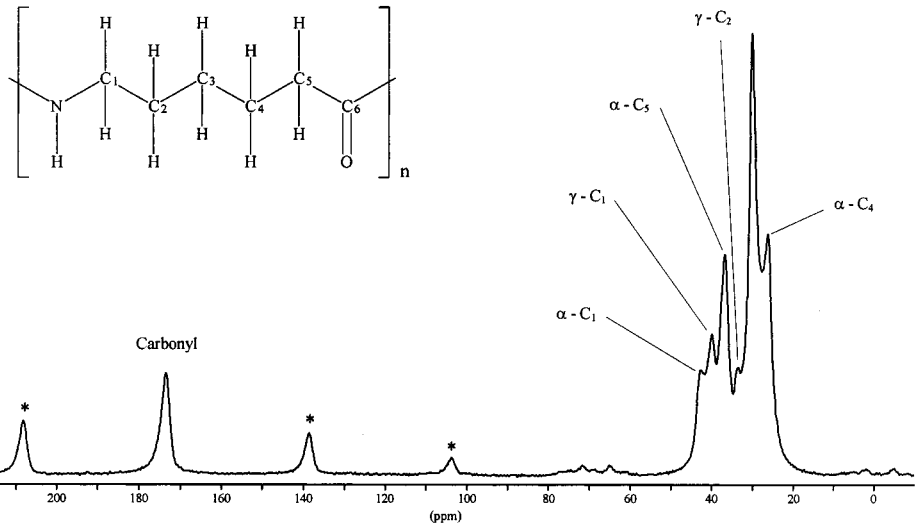

Figure 3. ^{13}C CPMAS spectrum of an undrawn polyamide-6 fiber and the assignment of some of the peaks. Spinning sidebands are marked with asterisks.

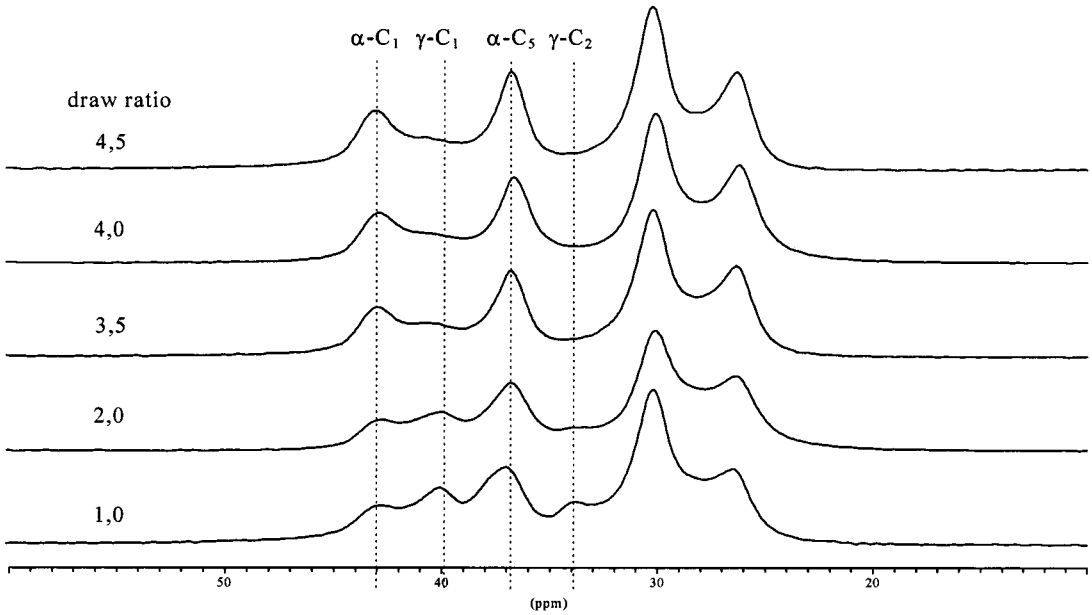

Figure 4. CH_2 resonances of ^{13}C CPMAS spectra of differently drawn polyamide-6 fibers.

given in the literature.[9,10] All resonances have a Lorentzian line shape. The obtained peak parameters (chemical shift and line width) for the α-phase were set to fixed values in a fitting analysis of the ^{13}C spectrum of the undrawn fiber which has the highest amount of γ-phase (see Figure 5b). Only the amplitudes of the α-resonances were left free in this fitting analysis, and three additional peaks for the γ-phase were added in order to get a good fit (see Figure 5b). The obtained chemical shifts for the γ-phase are similar to those of Hatfield et al.[10] but differ from previously reported data.[9] The chemical shifts of the methylene carbons determined in this way for both crystalline phases are given in Table 1. With this procedure, it was possible to get a good fit for all spectra obtained via the ^{13}C T_1 filter, by varying only the amplitudes of the peaks. The $^{\alpha}/_{\gamma}$ ratio can be determined from the peak intensities of both the C_1 and C_5 carbons. The values obtained from both carbons were very similar (within approximately 3%). The relative amounts of both crystalline phases are plotted as a function of the draw ratio in Figure 6. As was already clear from the ^{13}C CPMAS spectra, it is obvious that the relative amount of α-crystalline phase increases continuously with increasing draw ratio while the amount of the γ-crystalline phase decreases. At a draw ratio of $\lambda = 4.5$, the γ-phase has been vanished completely.

3.2. Relaxation Time Measurements. To separate contributions from the amorphous (mobile) and crystalline (rigid) phase to the MAS intensities in the 2D rotorsynchronized MAS spectra, to be discussed below, we made use of their difference in NMR relaxation behavior. Since only the carbonyl resonances are considered in the orientation measurements, we studied the NMR relaxation behavior of these carbons. It was concluded that the ^{13}C $T_{1\rho}$ experiments give the best distinction between the mobile and rigid phase. The results of the ^{13}C $T_{1\rho}$ experiments are given in Table 2.

The assignment of the ^{13}C $T_{1\rho}$ relaxation times to the mobile and rigid phases was based on line width considerations. It was found that the carbonyl resonance of the rigid phase has a smaller line width (~170 Hz) than that of the mobile phase (~300 Hz). After spin locking the carbons for 30 ms in a $T_{1\rho}$ experiment, the

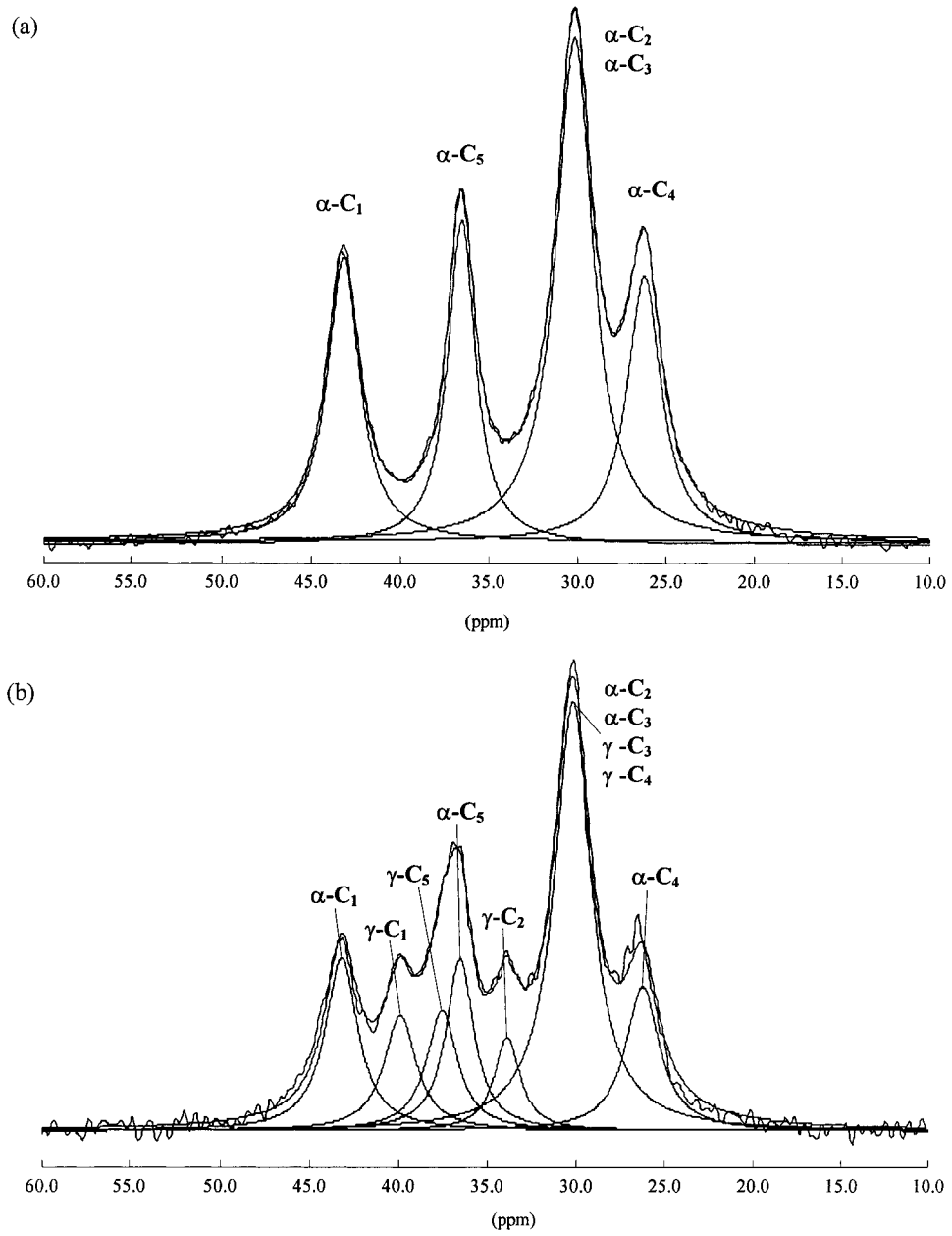

Figure 5. Deconvoluted CH_2 resonances of a spectrum obtained via ^{13}C T_1 filter of (a) a fiber drawn with a draw ratio of $\lambda = 4.5$, which is predominantly α, and (b) an undrawn fiber, which has a relatively high γ-phase content.

Table 1. ^{13}C Chemical Shifts of the Methylene Carbons in both Crystalline Phases of Polyamide-6

	chemical shift [ppm]				
phase	C_1	C_2	C_3	C_4	C_5
α	43.2	30.2	30.2	26.2	36.5
γ	39.9	33.9	30.2	30.2	37.5

remaining carbonyl signal has a peak width of approximately 170 Hz and can therefore be assigned to the rigid phase. We therefore attribute the short relaxation time (∼2−3 ms) to the mobile carbons and the long one (∼60 ms) to the rigid carbonyl carbon spins. This means that a selective detection of the rigid phase is possible by applying a 30 ms ^{13}C spin-lock pulse after cross polarization.

Before we discuss the orientation measurements, we will briefly discuss the results of the NMR relaxation measurements in more detail. With increasing draw ratios, the ^{13}C $T_{1\rho}$ relaxation times for the rigid phase increase slightly, while the relaxation times for the mobile phase seem to decrease slightly, especially at higher draw ratios ($\lambda > 3.5$). Temperature-dependent

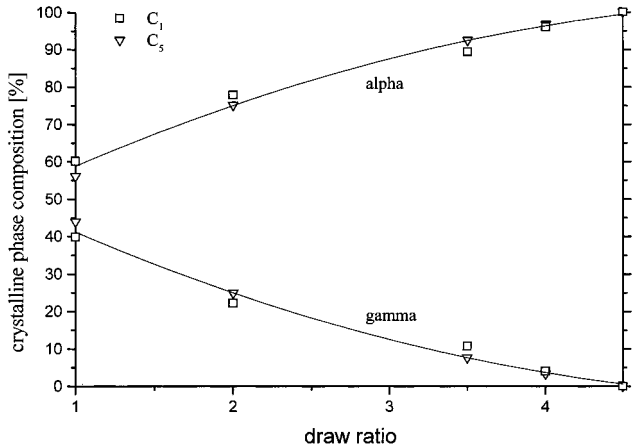

Figure 6. Change of crystal structure upon drawing.

Table 2. Results of the Carbonyl ^{13}C $T_{1\rho}$ Relaxation Time Measurements

draw ratio λ	$T_{1\rho}$ time, rigid [ms]	$T_{1\rho}$ time, mobile [ms]	rigid fraction [%]	mobile fraction [%]
1.0	55.0 ± 2.1	2.8 ± 0.3	73.3 ± 1.4	26.7 ± 1.4
2.0	56.3 ± 2.0	2.8 ± 0.3	75.8 ± 1.3	24.2 ± 1.3
3.5	58.6 ± 2.4	2.8 ± 0.4	78.4 ± 1.5	21.6 ± 1.5
4.0	59.1 ± 2.4	2.6 ± 0.3	74.0 ± 1.3	26.0 ± 1.3
4.5	65.5 ± 2.0	2.1 ± 0.4	84.6 ± 1.1	15.4 ± 1.1

relaxation time measurements in the range of 20° − 80 °C showed that for the rigid phase an increase in $T_{1\rho}$ time is related to a decrease in mobility, while for the mobile phase a decrease in $T_{1\rho}$ time is related to a decrease in mobility. This means that the mobility in both the rigid and the mobile phases decreases with increasing draw ratios. The fraction of the rigid phase seems to increase slightly with increasing draw ratio from 73.3 to 84.6%.

3.3. Orientation Measurements. *3.3.1. ^{13}C 2D CPMAS Spectra.* As an example, the ^{13}C rotorsynchronized 2D CPMAS spectra of the undrawn fiber and the fiber with draw ratio 4.5 are shown in Figure 7. Each sideband is characterized by an index M in the F_1 (vertical) dimension and N in the F_2 (horizontal) dimension; the carbonyl center band is set to $(M, N) = (0, 0)$. All spectra obey the following symmetry rule:[13]

$$I_{M,\,N} = I_{-M,\,N\,-\,M}$$

which indicates a good overall performance of the 2D experiment.

The CH_2 resonances of the polyamide-6 fibers in the $M = 0$ slice overlap with the resonances of the used glue. However, the glue resonances are absent in the higher slices, due to the unoriented state of the glue.

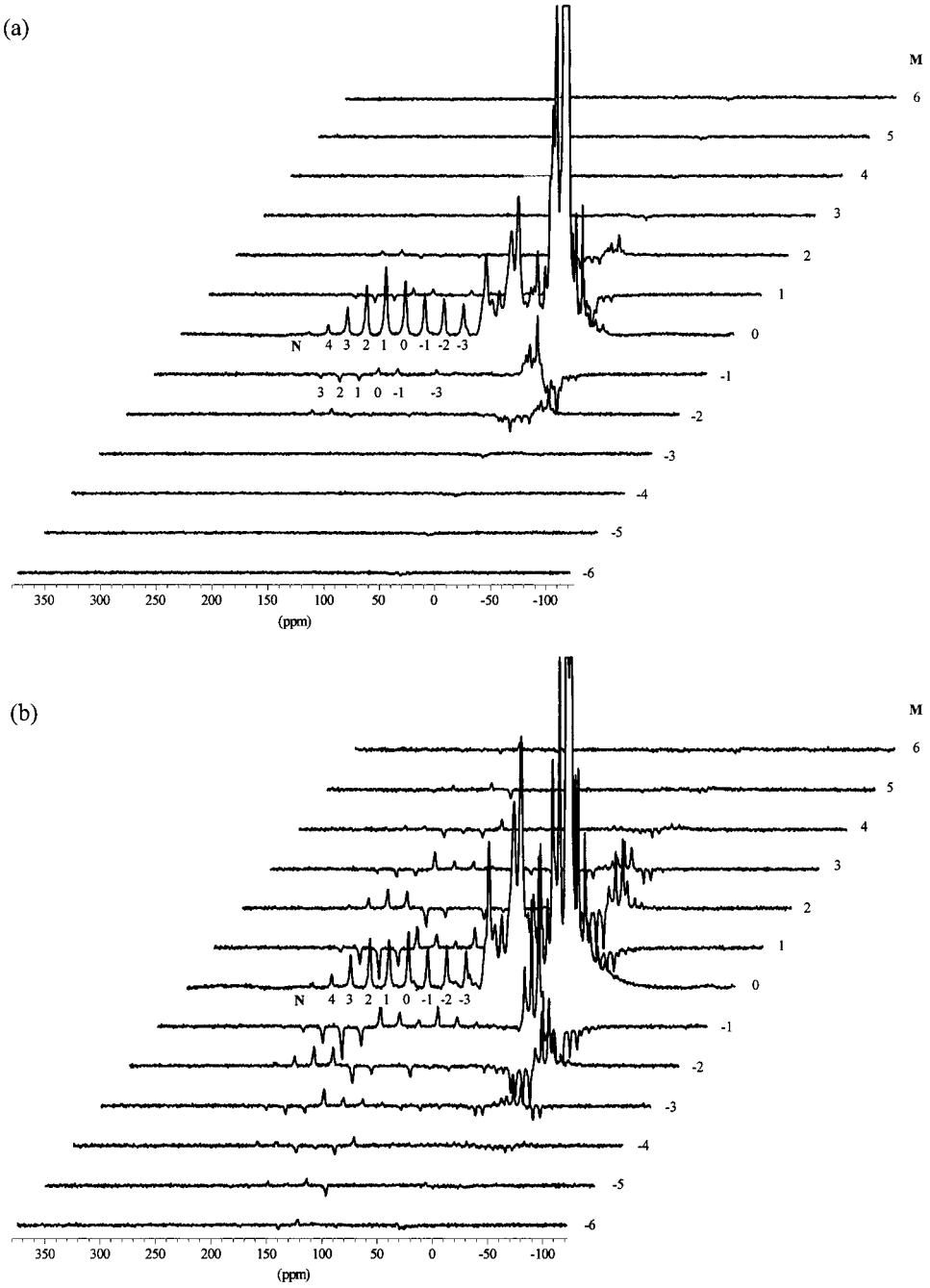

Figure 7. Rotorsynchronized ^{13}C 2D-CP/MAS spectra of (a) an undrawn fiber and (b) a fiber with draw ratio $\lambda = 4.5$.

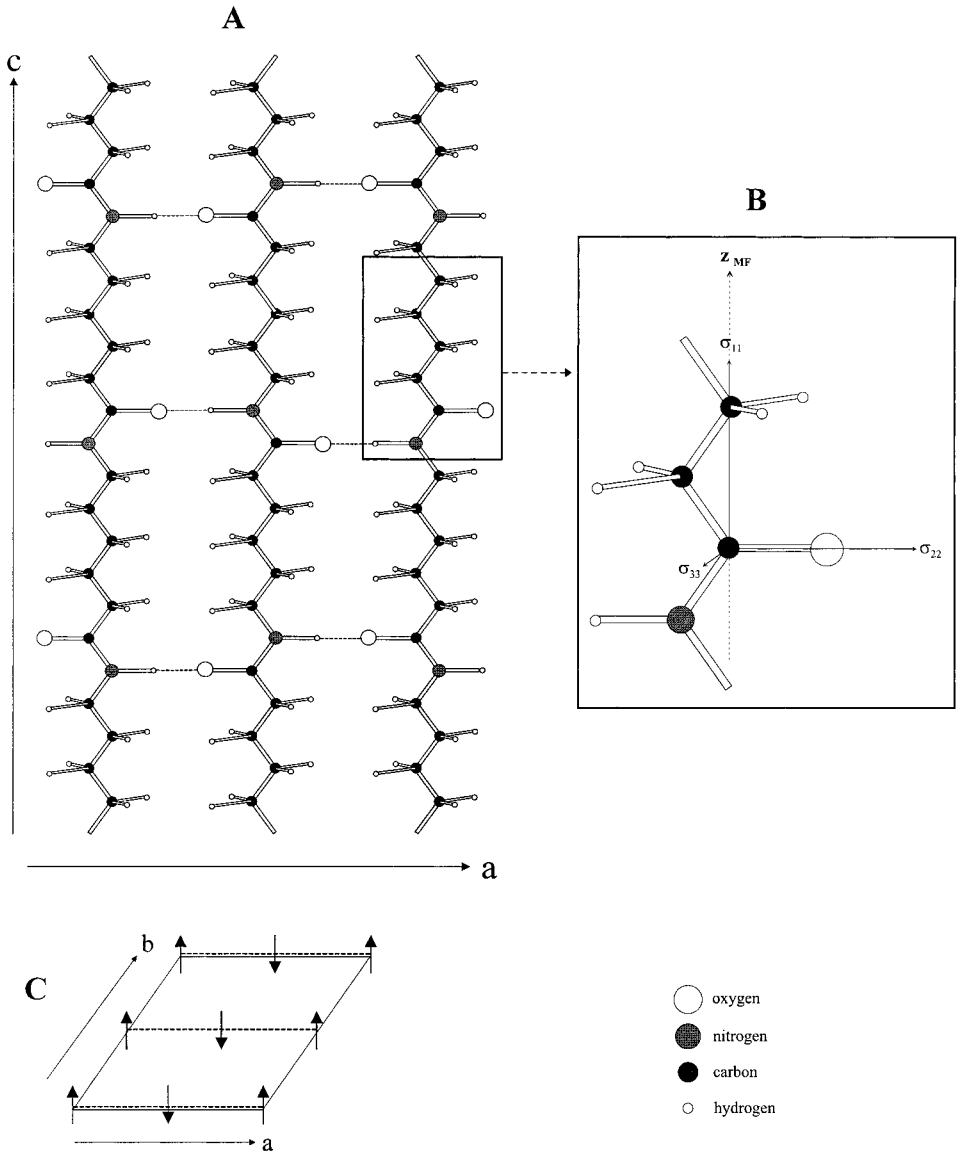

Figure 8. Schematic representation of the α-crystalline structure (A),[24] the carbonyl shielding tensor (B), and the basal plane (C). Hydrogen bonds are symbolized by dotted lines.

The 2D NMR spectra of the two fibers show clearly a different degree in orientation. For the undrawn fiber ($\lambda = 1.0$), carbonyl sideband intensities up to $M = \pm 2$ are found, while for the drawn fiber ($\lambda = 4.5$), intensities up to $M = \pm 6$ are visible, which indicates a much higher degree of orientation. The CH_2 resonances show a similar effect.

Before we discuss the results of the orientation measurements in terms of order parameters (section 3.3.3), we will first discuss the determination of the chemical shift tensor of polyamide-6 in the next paragraph, which is necessary for a good data analysis of the rotorsynchronized 2D spectra.

3.3.2. Chemical Shift Tensor of Polyamide-6. For an accurate determination of the order parameters from the spinning sideband intensities of a 2D CPMAS experiment, the exact values of the chemical shift tensor of the carbonyl carbon (σ_{11}, σ_{22}, and σ_{33}) and the Euler angles (α_0, β_0, and γ_0), which characterize the orientation of the chemical shift tensor in the molecular frame (MF), have to be known. These values are input parameters for the calculation of the order parameters from the experimental spectra. This has been extensively discussed for poly(ethylene terephthate) fibers in previous publications.[19,20]

Chemical Shift Principal Values. In principle, the tensor values can be determined by a Herzfeld−Berger analysis.[21] In this fitting procedure, σ_{11}, σ_{22}, and σ_{33} are calculated from the spinning sideband intensities of a one-dimensional ^{13}C CPMAS spectrum of a powder. Therefore, the fibers were cut into short pieces and loaded into the rotor. It appeared, however, that the small fiber pieces under spinning are not completely randomly distributed in the rotor (unlike a powder), and hence the calculated tensor values from the Herzfeld−Berger analysis are not accurate and can only be used as starting values in a fit. We therefore choose to fit the tensor values and the Euler angles directly from the ^{13}C rotorsynchronized 2D CPMAS spectrum.[20] This procedure yielded similar carbonyl tensor values for all fibers: $\sigma_{11} = 241.4$ ppm, $\sigma_{22} = 183.9$ ppm, and $\sigma_{33} = 94.2$ ppm. The error is estimated to be within 4%.

Euler Angles. The Euler angles (α_0, β_0, and γ_0) characterize the orientation of the chemical shift tensor in the molecular frame. For the definition of the Euler angle rotations, we use the definitions of Rose.[22] The

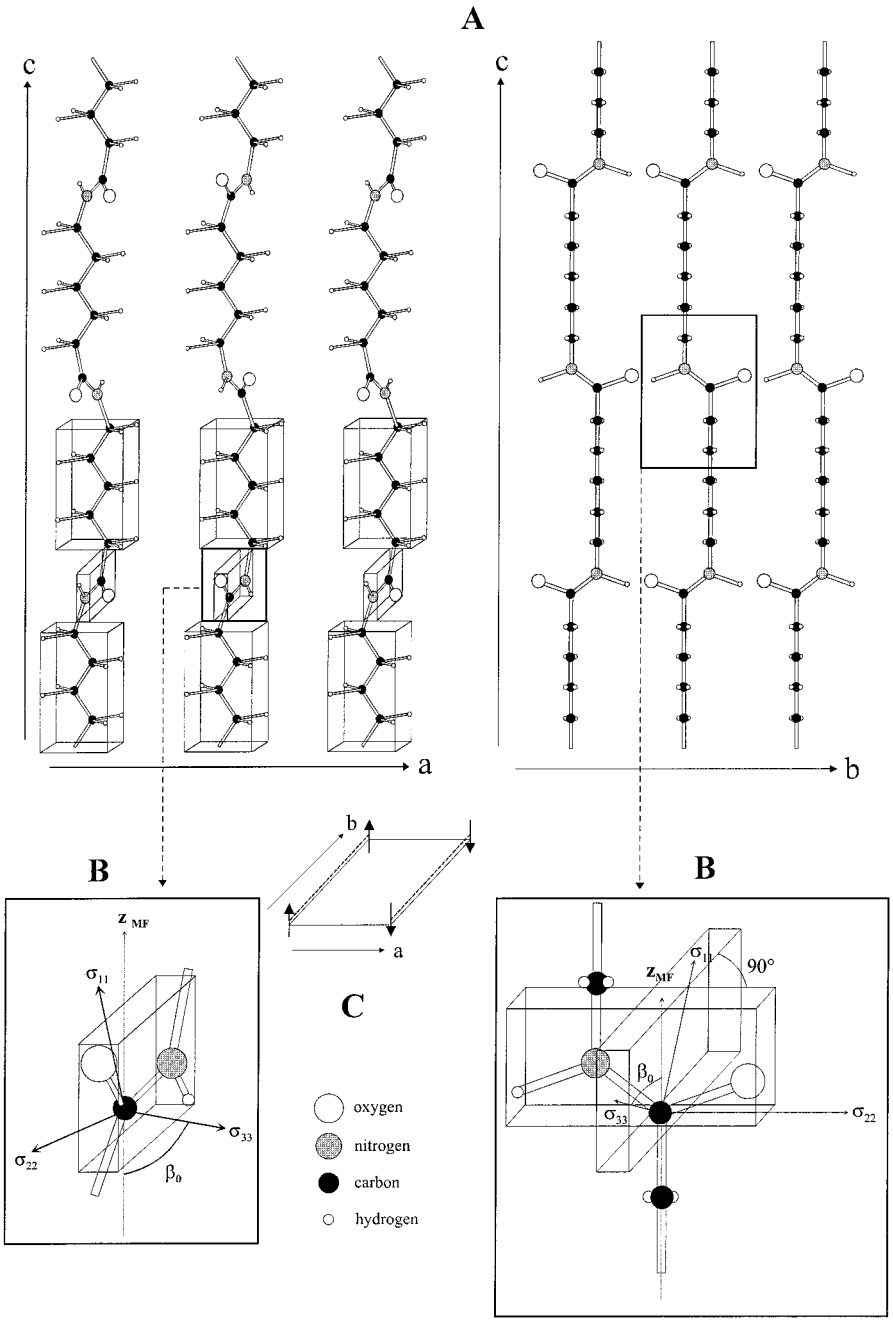

Figure 9. Schematic representation of the γ-crystalline structure (A),[25,26] the carbonyl shielding tensor (B), and the basal plane (C). Hydrogen bonds are symbolized by dotted lines.

MF can in principle be arbitrarily chosen with respect to the molecule. We choose the chain axis as the *z*-axis of the MF. For the conformation of polyamide-6, we want to use the conformation of polyamide-6 in the crystalline regions. However, two types of crystalline modifications for polyamide-6 exist for which the carbonyl chemical shift tensor will have different orientations. Since we cannot distinguish between carbonyl carbons of the α- and γ-phase in a ^{13}C spectrum, a single tensor orientation has to be assumed which will be an average of the α-, γ-, and the amorphous phases.

A schematic drawing of the α- and γ-crystalline structures in polyamide-6 fibers are shown in Figures 8 and 9, together with the carbonyl tensor orientations (obtained from our fitting results). The molecules in the monoclinic α-structure are in the extended flat zigzag configuration. The hydrogen bonds are formed between antiparallel chains. The basal plane of the monoclinic γ-structure is similar to the α-structure, but the hydrogen bonds are formed between parallel chains. To form the maximum number of hydrogen bonds, the amide group is forced to rotate such that the peptide plane is no longer parallel to the plane formed by the CH_2 groups. Therefore, the γ-crystalline phase has a shorter (about 2%) unit cell than the thermodynamically more stable α-form.[7]

Normally, σ_{11} and σ_{22} of the carbonyl tensor lie in the peptide plane, where σ_{22} is directed along the C═O bond or makes a small angle with the C═O bond[23] and σ_{33} is directed perpendicular to that plane. The Euler transformations have to be performed in such a way that σ_{33} becomes parallel to the chain axis.

By fitting the 2D spectra, it was found that the Euler angle α_0 is zero for all samples independent of the draw ratio, which indicates that σ_{22} is directed perpendicular to the chain axis independent of the structure (see

Table 3. Changes in Euler Angle β_0 with Draw Ratio

	draw ratio λ				
	1.0	2.0	3.5	4.0	4.5
overall β_0 [°]	64	78	86	90	90
rigid phase β_0 [°]	64	80	86	90	86

Table 4. Results of the Orientation Measurements; Overall Orientation (Rigid + Mobile)

draw ratio λ	$\langle P_2 \rangle$	$\langle P_4 \rangle$	$\langle P_6 \rangle$
1.0	0.21		
2.0	0.41	0.14	
3.5	0.63	0.36	0.28
4.0	0.61	0.37	0.27
4.5	0.69	0.44	0.36

Figures 8 and 9). For the α-crystalline phase, this means that σ_{22} is directed parallel to the C═O bond (see Figure 8 B). For the γ-crystalline phase, the σ_{22} axis must make an angle with the C═O bond (see Figure 9 B).

The Euler angle β_0 represents the angle between the carbonyl chemical shift principal axis σ_{33} and the *z*-axis of the molecular frame, the chain axis (Figures 8 and 9). The values of β_0 are given in Table 3. Most interestingly, the Euler angle β_0 changes from 64° for the undrawn fiber, which has a relative high amount of γ-crystalline phase (about 40%), to nearly 90° for the fiber with the highest draw ratio, which is rich in the α-phase (see Figure 6). Clearly, the change in β_0 is related to the change in crystal modification as shown before. In the α-crystalline phase, the peptide plane (O−C−N−C) is parallel to the chain axis (Figure 8). This means that in the α-crystalline modification ($\lambda = 4.5$) σ_{33} is directed perpendicular to the peptide plane ($\beta_0 =$ 90°), as is usual for amino acids. In the γ-crystalline structure, the peptide plane is tilted with respect to the CH_2 zigzag plane and assuming that the σ_{33} axis is perpendicular to the peptide plane it is no longer perpendicular to the chain axis, as was indeed revealed by the determined β_0 value ≠90°. It should be noted that the undrawn fiber for which a β_0 value of 64° was found still contains a substantial amount of α-crystalline phase. As pointed out before, the β_0 value we found is an average over both crystalline phases and the amorphous phase. So, only for a polyamide-6 fiber which is predominantly γ, can information about the tensor orientation in the γ-phase be obtained with this method. We estimate an error of about 5° in the determination of the angle β_o.

Finally, the Euler angle γ_0, which in principle can have any value between 0° and 360° due to the fiber symmetry of the system, was set to 0°. So, for the final analysis of the 2D MAS intensities we set $\alpha_0 = 0°$ and $\gamma_0 = 0°$, while the β_0 value which is related to the crystalline phase composition, was left free in the fitting procedure.

3.3.3. Order Parameters. The order parameters $\langle P_L \rangle$ have been determined by fitting the experimental spinning sideband intensities with the orientation distribution function $f(\theta)$:

$$f(\theta) = \sum_L \frac{(2L+1)}{2} \langle P_L \rangle P_L(\cos\theta)$$

where $P_L(\cos\theta)$ are the even Legendre functions.

The results of the overall orientation measurements are shown in Table 4. It is obvious that the overall orientational order increases with increasing draw ratio: $\langle P_2 \rangle = 0.21$ for the undrawn fiber up to 0.69 for the fiber with the highest draw ratio. The higher the degree of orientation, the more order parameters can be calculated from the spectra. Order parameters up to $\langle P_6 \rangle$ were determined for the most oriented sample. The error in the lower rank order parameters (P_2, P_4) is estimated to be <5%. Evidently, the error is larger (5−10%) in the higher rank order parameters.

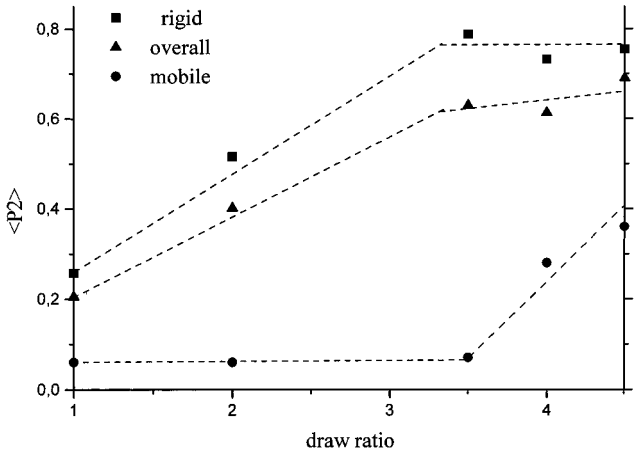

Figure 10. Effect of drawing on the orientational order parameter $\langle P_2 \rangle$.

Table 5. Results of the Orientation Measurements; Rigid Fraction and Calculated Mobile Fraction

	experimentally determined for rigid fraction			calculated for mobile fraction
draw ratio, λ	$\langle P_2 \rangle$	$\langle P_4 \rangle$	$\langle P_6 \rangle$	$\langle P_2 \rangle$
1.0	0.26			0.06
2.0	0.52	0.20	0.11	0.06
3.5	0.79	0.49	0.25	0.07
4.0	0.73	0.42	0.26	0.28
4.5	0.75	0.52	0.41	0.36

The relaxation measurements have shown that it is possible to detect the pure rigid phase using a carbon $T_{1\rho}$ filter, i.e., spin locking the carbons for 30 ms after cross polarization. A direct observation of the mobile phase is in principle possible by using carbon T_1 (short recycle delay) or proton T_2 filters. Due to the resulting low signal-to-noise ratios for both experiments, an accurate determination of the order parameters could not be achieved. However, the order parameters of the mobile phase can be calculated if the fractions of rigid and mobile phases are known. The order parameters are then given by

$$\langle P_L \rangle_{\text{overall}} = f_{\text{rigid}} \langle P_L \rangle_{\text{rigid}} + (1 - f_{\text{rigid}}) \langle P_L \rangle_{\text{mobile}} \qquad L = 0, 2, 4, \ldots$$

with $\langle P_L \rangle_{\text{overall}} = \langle P_L \rangle$, value as determined for the whole sample (rotorsynchronized 2D CPMAS experiment, Figure 2a); $\langle P_L \rangle_{\text{rigid}} = \langle P_L \rangle$, value of the rigid fraction (rotorsynchronized 2D CPMAS experiment with additional spin-lock pulse of 30 ms, Figure 2b); $\langle P_L \rangle_{\text{mobile}} = \langle P_L \rangle$, value of the mobile fraction (to be calculated); and f_{rigid} = rigid fraction (determined via ^{13}C $T_{1\rho}$ experiment, see Table 1). Although we found that the CP efficiencies for the rigid and mobile fractions are close, the fraction f_{rigid} determined via the ^{13}C $T_{1\rho}$ experiment is not completely accurate. However, since the overall $\langle P_L \rangle$ is made with the same CP experiments, it also is affected by the underestimation of the mobile

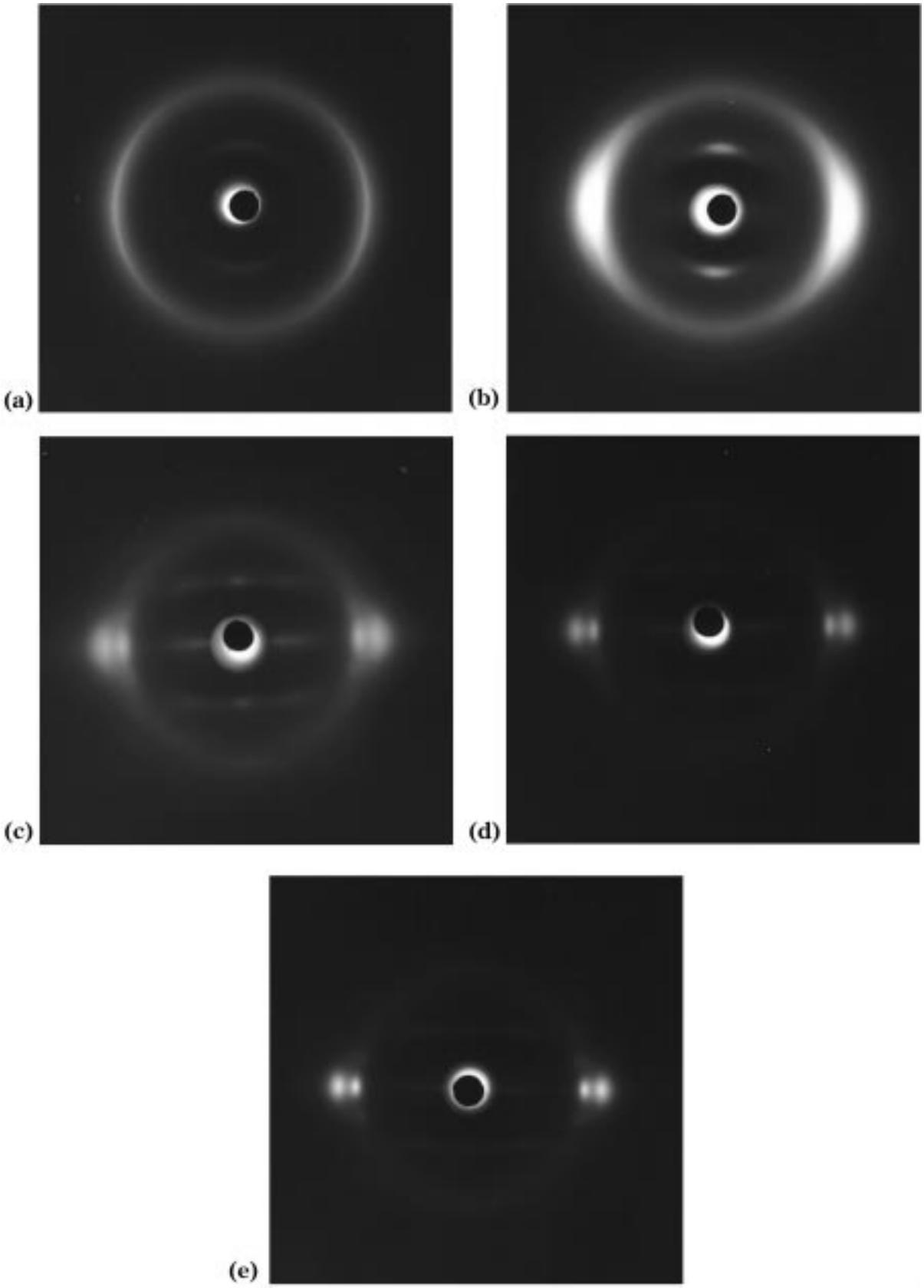

Figure 11. WAXS photos of an undrawn fiber (a) and of drawn fibers with draw ratio 2.0 (b), 3.5 (c), 4.0 (d), and 4.5 (e).

phase. That means that with the procedure as described $\langle P_L \rangle_{\text{rigid}}$ and $\langle P_L \rangle_{\text{mobile}}$ are independent of unequal CP efficiencies of the rigid and mobile phase. The $\langle P_L \rangle_{\text{overall}}$ values, however, are somewhat greater than they would be if the unequal CP rates would be taken into account.

Due to the low orientation in the mobile phase and the larger error in the higher rank order parameters, we have only calculated $\langle P_2 \rangle$ for the mobile phase. The results are shown in Table 5. The order parameters $\langle P_2 \rangle$ as a function of draw ratio of each fraction are plotted

in Figure 10. Obviously for each phase, the orientation of the polymer chains in the fibers increases with increasing draw ratios. The orientation of the rigid phase increases rapidly at low draw ratios up to a draw ratio of $\lambda = 3.5$ and remains practically constant at higher draw ratios. The mobile amorphous phase behaves differently. At low draw ratios up to $\lambda = 3.5$, the mobile amorphous phase remains disordered, whereas at higher draw ratios ($\lambda > 3.5$), the orientation in this phase increases rapidly. These results show that the increase in overall orientation at draw ratios $\lambda > 3.5$ is not related to an increase in orientation of the rigid crystallites but of the formerly disordered mobile amorphous phase. Note that these results are consistent with the NMR relaxation data, which show that the mobility of the mobile amorphous phase decreases at draw ratios $\lambda > 3.5$.

Our results suggest that the effect of drawing on orientation in polyamide-6 fibers can be described as follows. First, the rigid crystalline parts get oriented until they reach their maximum orientation. Further drawing results in an increase in orientation of the formerly unoriented mobile amorphous phase. The γ- to α-phase conversion upon drawing seems to be a continuous process and takes place even at low drawing ratios (see Figure 6).

Tzou et al.[11] obtained comparable results for the overall orientation as a function of drawing, but in addition, we were able to separate the contributions of the rigid and mobile phase to the overall orientation. Murthy and Bray[5] were able to determine the chain orientation order parameter $\langle P_2 \rangle$ for the crystalline domains and for the anisotropic (oriented) part of the amorphous domains using wide-angle X-ray spectroscopy (WAXS). They found that the orientation in the crystalline domains increased quickly up to draw ratios of $\lambda = 3$ and then reached a plateau which is similar to our NMR results for the rigid phase and to the results by Gianchandani et al.[8] The orientation of the anisotropic amorphous part as determined by WAXS increased slower with drawing but also reached a plateau, at a lower orientation than the crystalline domains at drawing ratios of about $\lambda = 4$.

The high percentage of rigid fraction determined via the ^{13}C $T_{1\rho}$ (Table 2) suggests that the rigid fraction not only is composed of crystalline domains, but that a rigid amorphous fraction with lower orientation is also involved. Consequently, the order parameters obtained for the crystalline phase by WAXS are always higher than the order parameters of the rigid phase as determined by NMR. In addition to information which confirms earlier results, our NMR results provide exclusive information about the degree of order in the mobile (relatively low-oriented) amorphous phase. It appears that this mobile phase does not remain disordered but gets oriented at high draw ratios ($\lambda > 3.5$).

The same fibers we investigated by NMR were also subjected to WAXS experiments. The WAXS pictures are shown in Figure 11. The evaluation of the WAXS data is not trivial due to overlapping of reflections. As an example, Figure 11a shows the reflections for an undrawn fiber. Although we know from the NMR results that two crystalline phases and one amorphous phase are present, only one reflection is observed. At higher draw ratios, two reflections in the equatorial plane appear, which, according to Heuvel and Huisman, can be assigned to the α-crystalline structure. A complete analysis of the WAXS data, following the model the model of Heuvel and Huisman,[2,27] will be published later; here, we discuss the WAXS data qualitatively. In agreement with NMR, it is shown in Figure 11a that the undrawn fiber has a low molecular orientation. In addition, the WAXS pictures show qualitatively an increased orientation with increasing draw ratio and the orientation seems to level off at higher ratios.

4. Conclusion

It has been shown that upon drawing various structural changes in polyamide-6 yarns take place. By using ^{13}C NMR filter methods it, was possible to study selectively the orientation in the mobile amorphous and in the rigid (crystalline) phase. The crystalline orientation increases rapidly at low draw ratios up to a draw ratio of $\lambda = 3.5$ and remains practically constant at higher draw ratios. The mobile amorphous phase behaves differently. At low draw ratios up to $\lambda = 3.5$, the amorphous phase remains disordered, whereas at higher draw ratios ($\lambda > 3.5$), the orientation in the amorphous phase increases rapidly. By using a T_1 filter, a ^{13}C MAS spectrum of the crystalline phase could be obtained from which the $^{\alpha}/_{\gamma}$ ratio could be determined. It appears that the crystalline phase composition ($^{\alpha}/_{\gamma}$) changes from $^{60}/_{40}$ for the undrawn yarn to $\sim^{100}/_{0}$ for the drawn yarn at a draw ratio of $\lambda = 4.5$.

Acknowledgment. We thank Dr. C. Versluis for helpful discussions.

References and Notes

(1) Prevorsek, D. C.; Harget, P. J.; Sharma, R. K.; Reimschuessel, A. C. *J. Macromol. Sci.-Phy.* **1973**, *B8* (1−2), 127−156.
(2) Heuvel, H. M.; Huisman, R.; Lind, K. C. J. B. *J. Polym. Sci., Polym. Phys. Ed.* **1976**, *14*, 921−940.
(3) Huisman, R.; Heuvel, H. M. *J. Polym. Sci., Polym. Phys. Ed.* **1976**, *14*, 941−954.
(4) Murthy, N. S.; Bednarcyk, C.; Moore, R. A. F.; Grubb, D. T. *J. Polym. Sci., Part B: Polym. Phys.* **1996**, *34*, 821−835.
(5) Murthy, N. S.; Bray, R. G. *Polymer* **1995**, *36* (20), 3863−3873.
(6) Murthy, N. S.; Aharoni, S. M.; Szollosi, A. B. *J. Polym. Sci., Polym. Phys. Ed.* **1985**, *23*, 2549−2565.
(7) Heuvel, H. M.; Huisman, R. *J. Appl. Polym. Sci.* **1981**, *26*, 713−732.
(8) Gianchandani, J.; Spruiell, J. E.; Clark, E. S. *J. Appl. Polym. Sci.* **1982**, *27*, 3527−3551.
(9) Weeding, T. L.; Veeman, W. S.; Angad Gaur, H.; Huysmans, W. G. B. *Macromolecules* **1988**, *21*, 2028−2032.
(10) Hatfield, G. R.; Glans, J. H.; Hammond, W. B. *Macromolecules* **1990**, *23*, 1654−1658.
(11) Tzou, D. L.; Spiess, H. W.; Curran, S. *J. Polym. Sci., Part B: Polym. Phys.* **1994**, *32*, 1521−1529.
(12) Harbison, G. S.; Spiess, H. W. *Chem. Phys. Lett.* **1986**, *124* (2), 128−134.
(13) Harbison, G. S.; Vogt, V. D.; Spiess, H. W. *J. Chem. Phys.* **1987**, *86* (3), 1206−1218.
(14) Subramanian, D. R.; Venkataraman, A. *J. Macromol. Sci.-Phy.* **1980**, *B18* (2), 177−193.
(15) Frank, B.; Frübing, P.; Pissis, P. *J. Polym. Sci., Part B: Polym. Phys.* **1996**, *34*, 1853−1860.
(16) Stuart, B. H. *Polym. Bull.* **1994**, *33*, 681−686.
(17) Jin, X.; Ellis, T. S.; Karasz, F. E. *J. Polym. Sci., Polym. Phys. Ed.* **1984**, *22*, 1701−1717.
(18) Khanna, Y. P.; Kuhn, W. P.; Sichina, W. J. *Macromolecules* **1995**, *28*, 2644−2646.
(19) Gabriëlse, W.; Angad Gaur, H.; Veeman, W. S. *Macromolecules* **1996**, *29* (11), 4125−4133.
(20) Gabriëlse, W.; van Well, H. F. J. M.; Veeman, W. S. *Solid State NMR* **1996**, *6*, 231.
(21) Herzfeld, J.; Berger, A. E. *J. Chem. Phys.* **1980**, *73* (12), 6021−6026.
(22) Rose, M. E. In *Elementary Theory of Angular Momentum*; John Wiley & Sons: New York, 1957; Chapter 1.

(23) Veeman, W. S. *Prog. Nucl. Magn. Reson. Spectrosc.* **1984**, *16*, 193.
(24) Holmes, D. R.; Bunn, C. W.; Smith, D. J. *J. Polym. Sci.* **1955**, *17*, 159−177.
(25) Arimoto, H.; Ishibashi, M.; Hirai, M. *J. Polym. Sci.* **1965**, *A3*, 317−326.
(26) Arimoto, H. *J. Polym. Sci.* **1964**, *A2*, 2283−2295.
(27) Heuvel, H. M.; Huisman, R. *J. Polym. Sci., Polym. Phys. Ed.* **1981**, *19*, 121−134.

MA9818679